Scripta Materialia 127 (2017) 37–40

Contents lists available at ScienceDirect

Scripta Materialia

journal homepage: www.elsevier.com/locate/scriptamat

Regular Article

On the composition of microtwins in a single crystal nickel-based superalloy

D. Barba[a], S. Pedrazzini[b], A. Vilalta-Clemente[b], A.J. Wilkinson[b], M.P. Moody[b], P.A.J. Bagot[b], A. Jérusalem[a], R.C. Reed[a,b,*]

[a] Department of Engineering Science, University of Oxford, Parks Road, Oxford OX1 3PJ, United Kingdom
[b] Department of Materials, University of Oxford, Parks Road, Oxford OX1 3PH, United Kingdom

ARTICLE INFO

Article history:
Received 9 June 2016
Received in revised form 4 August 2016
Accepted 23 August 2016
Available online 8 September 2016

Keywords:
Ni-based superalloy
Twinning
Transmission Kikuchi diffraction
Atom probe tomography

ABSTRACT

Correlative analysis is performed using atom probe tomography and high resolution transmission Kikuchi diffraction techniques on microtwins of ~10 nm thickness, in a ⟨011⟩-orientated single crystal superalloy crept at 800 °C and 650 MPa. Composition profiles across the microtwins and microtwin-parent boundaries are presented. Enrichment of microtwin-parent interfaces by approximately 2 at.% Cr and 1 at.% Co within the γ′-phase is found; no compositional variations of other elements – Ta, Nb, Mo, W – are detected. Our results provide unique insights into the mechanism of microtwin formation and the likely influence of alloy composition on deformation kinetics.

Plasticity in nickel-based superalloys is most commonly associated with either athermal yielding at temperatures between ambient and ~700 °C, or alternatively time-dependent creep deformation at conditions beyond ~850 °C. The former is mediated by either weakly- or strongly-coupled pairs of dislocations whose motion is controlled by propagation through the γ′-particles [1–3], whereas the latter depends upon the circumvention of them by climb-assisted glide within the γ-matrix [4]. At temperatures between these two limits a mode of deformation has been reported recently [5–8] involving the propagation of so-called microtwins, by a mechanism which is not completely understood, somewhat controversial but also of significant practical importance.

Microtwins are caused by the propagation of 1/6⟨112⟩ twinning partials on every consecutive {111} plane [9]. Thus, the diffusion-assisted reordering needed in the vicinity of the leading partials for twin growth can provide a time-dependent character. These concepts have been discussed in the literature [5,6,10,11], especially in the work of Kovarik et al. [5] where the reordering process needed has been studied in detail using ab initio atomistic calculations. However, the latest results obtained using high angle annular dark field imaging [12–15] have revealed a further intriguing aspect of this deformation mode, since the planar faults formed in this region have been found to support segregation of certain important alloying additions. Thus, local enrichment of Co and Cr – and depletion of Ni and Al – at planar faults in the CMSX-4 and ME3 alloys has been reported [12]. Furthermore, the segregation of Ta and W found at superlattice intrinsic stacking faults (SISFs) in a series of Co-based superalloys has been rationalised by means of the phase transformation $\gamma' \rightarrow Co_3Ti$ [13]. Similarly, segregation of Co, Ta, Nb and Ti at superlattice extrinsic stacking faults (SESFs) in ME3 – and again depletion of Ni and Al – have been reported [14]. There, the presence of a solute atmosphere – rich in Cr and Co and lean in Ni and Al – surrounding the leading Shockley partials was detected, suggesting that its diffusive movement in a viscous manner might be associated with the shearing process. Thus the idea that the microtwinning process exhibits characteristics of a coupled diffusional-displacive phase transformation has gathered pace in the last few years. But quantitative chemical analysis at atomic resolution is lacking.

Hence, improved high resolution chemical analysis is needed, to better understand the effects occurring and especially to support quantitative theory and modelling of this mechanism. For the present investigation, single crystal samples of the prototype nickel based superalloy MD2 [16] of composition Ni–11.2Al–9.3Co–5.3Cr–2.6W–2Ta–1.65Ti–1.33Mo–0.2Si–0.03Hf in at.% were investment cast into bars aligned along the ⟨011⟩ crystallographic axis. This orientation was chosen because Schmid factor analysis indicates that the microtwinning mode is then favoured. Solution treatment was carried out at 1275 °C for 8 h, followed by ageing for 6 h at 1080 °C

* Corresponding author at: University of Oxford, Dept. of Engineering Science, Parks Road, Oxford OX1 3PJ, United Kingdom.

http://dx.doi.org/10.1016/j.scriptamat.2016.08.029
1359-6462/

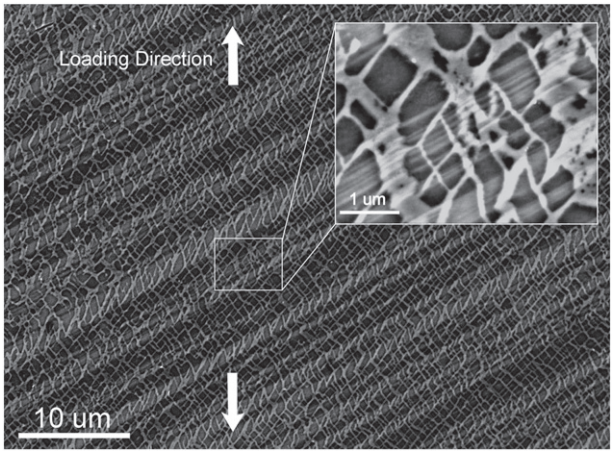

Fig. 1. SEM backscattered electron micrograph showing twin bundles and γ-γ'-phase distribution in MD2 alloy after creep testing at 800 °C and 650 MPa.

and finally at 870 °C for 16 h. Creep test pieces of gauge volume $16 \times 1.6 \times 1\text{mm}^3$ were used. The crept material characterised in this paper formed part of a broader creep testing campaign to assess the temperature and stress-dependence of the microtwin mechanism; it was deformed at 800 °C under an applied tensile load of 650 MPa, consistent with conditions in which microtwins are expected to appear [8,17]. Testing was conducted in an Instron electro-thermal mechanical testing (ETMT) machine with strain measurements performed by means of a non-contact extensometer.

Post-mortem examination was carried out after fracture using a Zeiss Merlin field emission gun scanning electron microscope (FEG-SEM) with a Gemini II column using an accelerating voltage of 10 kV and probe current of 300 pA. Backscattered electron images were acquired in order to exploit the channelling contrast provided by the change in orientation of the microtwins. An overview of the microtwins that formed is shown in Fig. 1. The γ'-precipitates are shown and they are of order 1 µm in size. The microtwins appear as diagonal bands of different contrast; they appear arranged in bundles, with thickness varying between 50 nm and 2 µm. Deformation of the γ-phase within the microtwin is also clearly visible as the γ'-precipitates are sheared inside the twinned regions.

Samples were prepared using a Zeiss NVision 40 focused ion beam microscope (FIB) for correlative atom probe tomography (APT)/transmission Kikuchi diffraction (TKD) analysis. A protective W capping layer was Ga beam deposited, then a $25 \times 4\mu\text{m}^2$ cantilever was machined out and extracted using a Kleindiek micromanipulator from site specific twinned regions. The cantilever was cut and mounted onto a Cameca standard flat-top Si coupon using W welds and sharpened until the apex of the sample did not exceed 100 nm in diameter. The axis of the needle was perpendicular to the tensile direction of the sample. A 45° pre-angled sample holder was custom made for the present analysis, which enabled the APT coupon to be loaded into a Zeiss Merlin SEM equipped with a Bruker EBSD system for TKD analysis. TKD was performed at 20 kV with a probe current of 300 pA, following a square grid with a minimum pixel size of 20 nm. Patterns were acquired from rectangular sections 2 µm in length, 80 nm in width following the length of the sample. Inverse pole figure maps showing the grain orientations were plotted using 20 nm length scale, and relative misorientation profiles were plotted along specific lines to ensure 60° rotations about the ⟨111⟩ axis were observed at the microtwin-parent interfaces [18]. Atom probe tomography was performed on the samples following TKD, using a Cameca Local Electrode Atom Probe (LEAP) 5000 XR. Samples were run using a UV laser with energy 100 pJ, frequency 160 kHz, and temperature −223 °C. Reconstructions were performed using IVAS 3.6.12 software. The correlative analysis is illustrated in Fig. 2.

Fig. 2 proves conclusively the presence of two microtwins in an atom probe needle prior to APT analysis. Fig. 2(a) illustrates the needle SEM micrograph and its associated TKD inverse pole figure map. Two microtwins are shown in the inverse pole figure map, and the misorientation profile along them is plotted in Fig. 2(b). Both microtwins exhibit a sharp 60° step, associated the microtwin-parent interfaces. Only misorientations <4° were recorded within the twin and the matrix domains themselves. Fig. 2(c) shows the corresponding APT maps which corresponds to the yellow region in the needle indicated in Fig. 2(a). Two γ-γ'-phase boundaries are shown, and four interfaces were detected within one of the γ'-precipitates. The crystallographic information provided by APT is in general rather limited; usually crystallographic features such as twins and stacking faults are not directly observable. However, their presence in an analysis can be indirectly detected by the observation of local segregation of solute atoms to these features. Furthermore, it is also well documented that such features can also be imaged indirectly in the form of regions of aberrantly high atom density in the 3D reconstruction [19,20]. These regions arise due to subtle aberrations in the trajectories of the field evaporated ions in the APT experiment itself, instigated by these microstructural features. In Fig. 2(c) analysis of the atomic density fluctuations through the APT clearly highlights the features interfaces. Furthermore, a vertical ⟨011⟩ pole is present along the axis of the needle, as shown by the TKD analysis, and corresponding atomic planes can be resolved within the 2D slice through the APT reconstruction presented in Fig. 3(a). These planes do not appear between the I1-I2 interfaces but are present

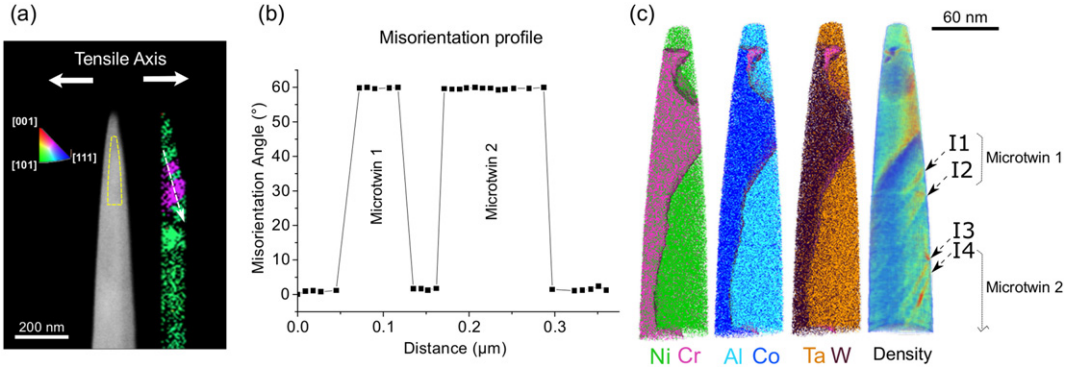

Fig. 2. (a) SEM secondary electron micrograph showing the atom probe needle and TKD inverse pole figure map plotted along the z-axis; (b) two regions displaying 60° misorientation angle corresponding to microtwins are shown to be present in the needle; (c) atom maps of the yellow region indicated in (a) created through the reconstruction of the APT data set, with γ-γ'-phase transitions shown as Ni–Cr, Al–Co and Ta–W partitioning.

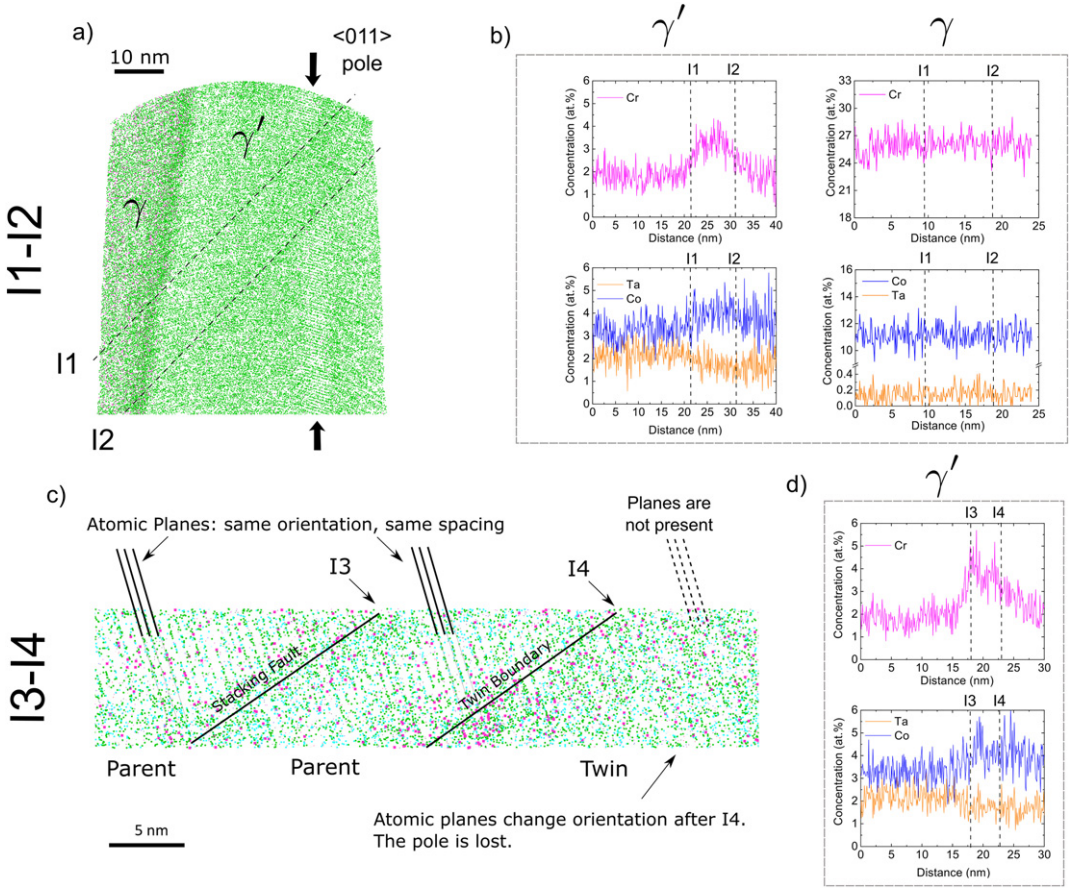

Fig. 3. Sub-section of the atom probe reconstruction shown in Fig. 2: (a) atomic planes are visible along the indicated ⟨011⟩ pole within the γ′-phase and interrupted inside the microtwin; (b) 1D concentration profiles of Cr, Co and Ta at the I1-I2 interfaces within the γ′-precipitates and the γ-matrix; (c) atom map detail of the region containing I3 and I4 interfaces, the crystal orientation is conserved across I3 but not across I4; (d) segregation of Cr and Co at the I3-I4 interfaces in the γ′-precipitate.

on either side of this region, which is consistent with the localised change in crystallographic orientation in the twin. At the I3 interface the planes are seen to remain continuous across the feature in the APT data as shown in Fig. 3(c) indicating that I3 is in fact a stacking fault. The atomic planes are again seen to be discontinuous at the I4 interface indicating another abrupt change of orientation at a twin boundary. Through the aforementioned correlation analysis, the following faulted structure can be inferred in Fig. 2(c) starting from the apex of the needle: first a microtwin is present between I1 and I2, then the parent material extends until I3, which from the pole analysis can be expected to be stacking fault, and then a second microtwin starts at I4. The segregation at the interfaces within the γ′-precipitate is shown in Fig. 3(b,d) as 1D chemical concentration profiles crossing each of the interfaces. The Cr content was shown to increase by 2 at.% and Co by 1 at.% at the microtwin-parent interfaces. The higher concentration of Cr at the interface leads to sharper peaks than in the case of Co. The very early stage of growth of the first microtwin (<20 nm) can explain the overlap of the two concentration peaks observed at I1 and I2. Furthermore, the different evaporation energies of the chemical species analysed here lead to slight changes of the segregated peaks between Cr and Co. Further analysis in other needles showed a clear separation between segregated peaks when the twin thickness increases. The thickness of the microtwin can be affected by these artefacts of the technique as well. In contrast, no chemical segregation was observed at the faults within the γ-matrix as shown in Fig. 3(b). These results constitute the first instance of quantitative chemical analysis performed on microtwin-parent interfaces formed in a nickel-based superalloy.

The elemental segregation detected indicates that the following mechanism for microtwin formation is operative, see Fig. 4. First, a pair of perfect $1/2[\bar{1}01](111)$dislocations arrive and get trapped at the γ-γ′-phase boundary, see Fig. 4(a). Second, these dislocations dissociate into partial dislocations, see Fig. 4(b), with differing Schmid factors; the partial $1/6[\bar{2}11]$ of higher Schmid factor enters the precipitate creating a high energy CSF behind it, thus preventing its extensive propagation into the γ′. Third, Co and Cr partition to the leading partial, see Fig. 4(c), thus lowering the energy of the CSF. The increase of Co and Cr at the nucleus of the fault would lead, at the limit of an FCC structure, to an extrinsic stacking fault in a γ-stabilised atmosphere, idea previously proposed by Smith et al. [14] for SESFs. At the same time the short range reordering after the fault leads to the twinned embryonic structure while the leading partials can continue shearing the precipitate, see Fig. 4(d). This process leaves behind them a trace of Co and Cr remnant from the shearing process, see Fig. 4(d). This involves long range diffusion and a continuous flux of Co and Cr to the advancing partials. The microtwin embryo thickens by a ledge mechanism, see Fig. 4(e), in a similar way as the one proposed recently by Smith et al. [21]. The partials shearing on every consecutive planes benefit from this remnant Cr and Co enriched regions. Notably, it is expected that the leading partials confer faster shear rates than might have been expected by long range diffusion alone [12]. Plausibly, the mature microtwin arising from this mechanism possesses segregation of Co and Cr at the microtwin-parent interfaces only or within close vicinity of them, see Fig. 4(f); there exists the possibility of slight enrichment of these elements inside the twin arising from the shearing partial residue. According

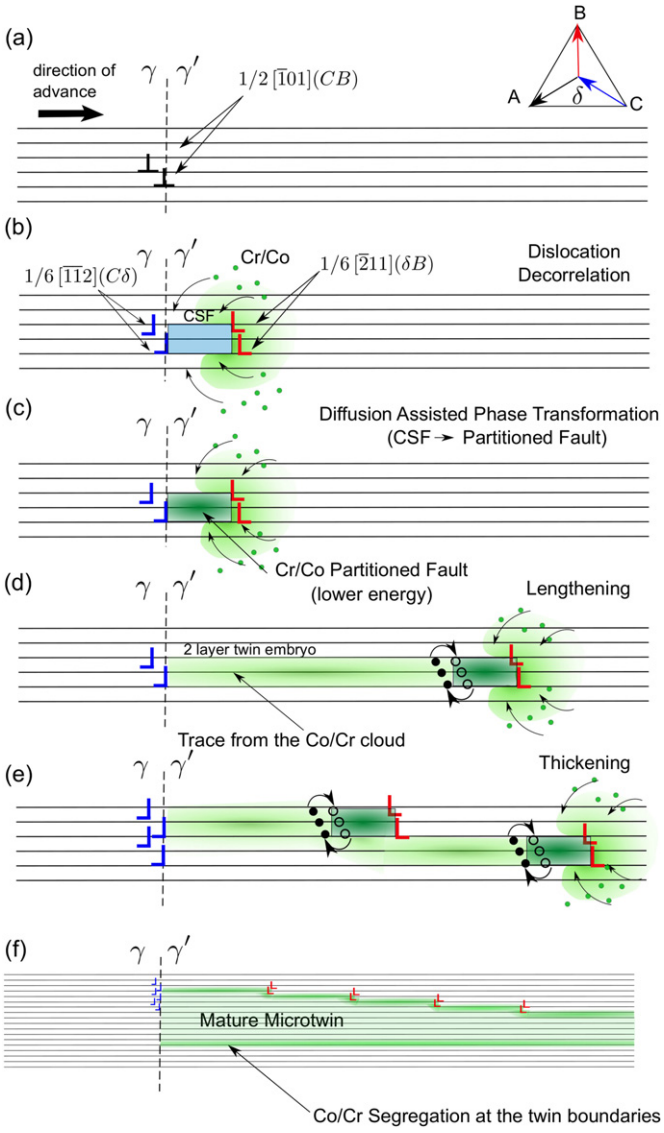

Fig. 4. Schematic illustration of the microtwinning mechanism: (a) perfect 1/2[$\bar{1}$01](111) dislocations get trapped at the γ/γ′-phase boundary; (b) partials 1/6[$\bar{2}$11] of higher Schmid factor (red) enter the precipitate creating a high energy CSF thus preventing their propagation; (c) long range diffusion Co and Cr enrichment at the fault lowers the energy of the fault, followed by short range atomic reordering results in a microtwin embryo; (d) the leading partials can now continue shearing the precipitate leaving behind them traces of Co and Cr; (e) the partials shear on every consecutives planes thus thickening the microtwin; (f) the mature microtwin contains segregation of Co and Cr at the microtwin-parent interfaces.

to the present hypothesis, the chemical alteration of the high energy fault just after the dislocations, and thus the long range diffusion of Co–Cr to the dislocations nuclei, may be the critical step for the twin lengthening, thus controlling the kinetics of the mechanism. This claim is also supported by the work of Viswanathan et al. [12] which suggests that the movement of partials during planar fault growth is controlled instead by the rate of diffusion of segregating elements. Furthermore, Smith et al. [14] proposed that segregation occurring at the fault tip has a localised stabilising effect, accomplished through the formation of a nanometre-sized region of γ-phase at the planar fault tip within the γ′-precipitates. The localised microtwinning partitioning of Cr and Co presented here (known γ-phase stabilising elements) supports this hypothesis. In conjunction with the long range diffusion-assisted dislocation shearing presented here, the short range reordering events proposed in early microtwin formation theories are still needed to form the final twinned atomic arrangement. Further modelling is required to fully understand the coupling between the short range reordering and the long range diffusion taking place simultaneously. It is however noteworthy that no relevant compositional changes of Ta, Nb, Mo, W or Ti have been found in our APT analysis, whereas some have been reported in previous cited studies performed on SESFs and SISFs [12–14]. This may be an effect of the crystallographic orientation ⟨011⟩ chosen for the present study, or a by-product of the selected testing mode (in tension rather than compression). More detailed analysis will be reported elsewhere due to space limitations here.

In summary, the first quantitative compositional analysis of microtwins in a single crystal nickel-based superalloy is reported. We have made correlative use of atom probe tomography and transmission Kikuchi diffraction. Our results indicate that microtwin formation, lengthening and thickening require the long range diffusion of critical elements such as Cr and Co, along with the previously studied short range reordering. Our findings provide critical and important data to support future quantitative modelling of the microtwinning mechanism, and the dependence of its kinetics upon alloy composition.

Acknowledgements

The authors are grateful to J. Moverare and M. Segersäll for the provision of material. The authors also thank P. Kontis for his assistance and advice during the experimental campaign. The Oxford Atom Probe facility was funded by the EPSRC grant EP/M022803/1. Funding from the EPSRC is acknowledged under grants EP/M50659X/1, EP/K032518/1 and EP/K032518/1.

References

[1] R.C. Reed, C.M.F. Rae, in: D.E. Laughlin, K. Hono (Eds.), Physical Metallurgy, Elsevier, Oxford, 2014, pp. 2215–2290.
[2] E.I. Galindo-Nava, L.D. Connor, C.M.F. Rae, Acta Mater. 98 (2015) 377–390.
[3] D.J. Crudden, A. Mottura, N. Warnken, B. Raeisinia, R.C. Reed, Acta Mater. 75 (2014) 356–370.
[4] T.M. Pollock, A.S. Argon, Acta Metall. Mater. 40 (1992) 1–30.
[5] L. Kovarik, R.R. Unocic, J. Li, P. Sarosi, C. Shen, Y. Wang, M.J. Mills, Prog. Mater. Sci. 54 (2009) 839–873.
[6] G.B. Viswanathan, P.M. Sarosi, M.F. Henry, D.D. Whitis, W.W. Milligan, M.J. Mills, Acta Mater. 53 (2005) 3041–3057.
[7] M. Legros, N. Clement, P. Caron, A. Coujou, Mater. Sci. Eng. A 337 (2002) 160–169.
[8] D.M. Knowles, S. Gunturi, Mater. Sci. Eng. A 328 (2002) 223–237.
[9] M. Kolbe, Mater. Sci. Eng. A 319-321 (2001) 383–387.
[10] S. Karthikeyan, R.R. Unocic, P.M. Sarosi, G.B. Viswanathan, D.D. Whitis, M.J. Mills, Scr. Mater. 54 (2006) 1157–1162.
[11] N. Zhou, C. Shen, M.J. Mills, J. Li, Y. Wang, Acta Mater. 59 (2011) 3484–3497.
[12] G.B. Viswanathan, R. Shi, A. Genc, V.A. Vorontsov, L. Kovarik, C.M.F. Rae, M.J. Mills, Scr. Mater. 94 (2014) 5–8.
[13] M.S. Titus, A. Mottura, G.B. Viswanathan, A. Suzuki, M.J. Mills, T.M. Pollock, Acta Mater. 89 (2015) 423–437.
[14] T.M. Smith, B.D. Esser, N. Antolin, G.B. Viswanathan, T. Hanlon, A. Wessman, D. Mourer, W. Windl, D.W. McComb, M.J. Mills, Acta Mater. 100 (2015) 19–31.
[15] J.F. Nie, Y.M. Zhu, J.Z. Liu, X.Y. Fang, Science 340 (2013) 957–960.
[16] D. Leidermark, J.J. Moverare, S. Johansson, K. Simonsson, S. Sjöström, Acta Mater. 58 (2010) 4986–4997.
[17] R.R. Unocic, N. Zhou, L. Kovarik, C. Shen, Y. Wang, M.J. Mills, Acta Mater. 59 (2011) 7325–7339.
[18] J.J. Moverare, S. Johansson, R.C. Reed, Acta Mater. 57 (2009) 2266–2276.
[19] M. Herbig, M. Kuzmina, C. Haase, R.K.W. Marceau, I. Gutierrez-Urrutia, D. Haley, D.A. Molodov, P. Choi, D. Raabe, Acta Mater. 83 (2015) 37–47.
[20] P.J. Felfer, B. Gault, G. Sha, L. Stephenson, S.P. Ringer, J.M. Cairney, Microsc. Microanal. 18 (2012) 359–364.
[21] T.M. Smith, R.R. Unocic, H. Deutchman, M.J. Mills, Materials at High Temperatures 33 (2016) 1–12.